CO_2 LASER WAVEGUIDING IN PROTON IMPLANTED GaAs

H. A. Jenkinson
US Army ARRADCOM, Dover, NJ 07801

D. C. Larson
Drexel University, Philadelphia, PA 19104

SUMMARY

Surface layers capable of supporting optical modes at 10.6 microns have been produced in n-type GaAs wafers through 300 keV proton implantation. The dominant mechanism for this effect appears to be free carrier compensation. Characterization of the implanted layers by analysis of infrared reflectivity spectra and synchronous coupling at 10.6 microns produce results in good agreement with elementary models.

INTRODUCTION

Integrated optical circuits have vast potential for use as sensing and signal processing elements in future Army fire control systems. One of the requirements for these systems is 24 hour/all weather operation. In order to meet this requirement, the Army has been emphasizing systems which operate at longer wavelengths, in particular, at the 10.6 micron CO_2 laser line. Such systems, including CO_2 laser radars, miss-distance sensors, and sensors for smart munitions, form a natural area of application for infrared integrated optical circuits. These circuits could be used to perform various functions including phased array transmission, heterodyne detection, parallel processing and optical correlation.

Methods which have been used to fabricate optical waveguides and components include thin film deposition, epitaxial growth, ion diffusion, and ion implantation. (ref. 1) The latter method is a particularly interesting technique that can produce electronic, chemical, and optical changes. In crystalline semiconductor materials, ion implantation can alter the refractive index through various physical mechanisms such as damage, doping, stress, and free carrier compensation. However, it is possible, by careful design of the implantation conditions to accentuate one of these mechanisms and to minimize the effects of the others. The present experiments are centered on free carrier compensation of highly doped n-type GaAs through medium energy proton implantation. Although this technique has been used to produce optical waveguides for use in the near infrared (ref. 2), little work has been done to investigate this effect for use at 10.6 microns.

This phenomenon can be illustrated by a simple dielectric model in which the dielectric function of GaAs is composed of Lorentz oscillator terms representing the lattice contribution (ref. 3) and a Drude term representing the depression of the dielectric function due to the presence of free carriers. (ref. 4) In the spectral region between the band gap and the IR phonon resonance, the dispersion due to the lattice contribution is much less than that due to the plasma for heavily doped material. Thus,to good approximation, the dielectric function for these

materials may be written, in terms of wavenumber σ, as

$$n^2(\sigma) = K_L - \frac{\sigma_p^2}{\sigma(\sigma + ig)} \qquad 269 \text{ cm}^{-1} \ll \sigma \ll 2\text{x}10^4 \text{ cm}^{-1} \tag{1}$$

where K_L is the high frequency dielectric constant of GaAs, taken to be 10.7. σ_p^2 is related to the carrier concentration N through

$$\sigma_p^2 = \frac{Ne^2}{(2\pi e)^2 m^* \varepsilon_o} \tag{2}$$

where e is the electronic charge, $m^* = .08m$ is the effective mass of electrons in GaAs, and ε_o is the vacuum permittivity. The damping factor, g, leads to losses and is related to the mobility, μ, of the material through

$$g = \frac{e}{2\pi c \mu m^*} \tag{3}$$

where c is the speed of light. During ion implantation, electronic trapping centers are created in the lattice which compensate the free carriers, effectively raising the refractive index. Neglecting losses, the increase in the refractive index is approximately

$$\Delta n \simeq \frac{\sigma_{p,s}^2 (1 - N_f/N_s)}{2n\sigma^2} \tag{4}$$

where $\sigma_{p,s}^2$ is σ_p^2 evaluated using the original carrier concentration N_s before implantation, and N_f is the carrier concentration remaining in the layer after implantation.

Polished (100) wafers of silicon doped GaAs were used in these experiments. The free carrier concentration was approximately $4\text{x}10^{18}/\text{cm}^3$. These wafers were implanted at room temperature with 300 keV protons to fluence levels from 10^{13} to $10^{16}/\text{cm}^2$. The implantation was performed at the Naval Research Laboratory. According to the LSS projected range calculations, the compensated region is expected to be sharply defined at a depth of approximately 3 microns. (ref. 5) Such a compensation profile would be unsuitable for optical waveguiding. However, it is experimentally observed that the implantation produces a damage layer with more uniform optical properties extending from near the surface to the projected range.

INFRARED REFLECTIVITY

Prior to waveguiding experiments the optical properties of the implanted sam-

ples were characterized by infrared reflectivity measurements. Differential reflectivity measurements, made over the spectral range of 4000 cm^{-1} to 800 cm^{-1}, yielded interference fringes typical of a thin film/substrate structure, as illustrated in figure 1. The interesting features of these curves are the periodicity of the fringes and their increase in amplitude as the measurement progresses to shorter wavenumbers. A first-order model has been developed to aid in deducing the compensation and the thickness of the implanted layer from the reflectivity spectrum. Basically, losses are neglected and the implanted layer is considered to be a film of refractive index n_f sitting atop a substrate whose index has been depressed a small amount Δn by its higher concentration of free carriers. The reference sample is considered identical to the substrate. Expanding the relevant reflectivity equations in a McLaurin series expansion to first order in Δn and using equation (4) yields

$$R_D^2(\sigma) = \frac{R^2_{sample}}{R^2_{reference}} \simeq 1 + \frac{4\sigma^2_{p,s}(1-N_f/N_s)}{n_f(n_f^2-1)}\left(\frac{\sin(2\pi t n_f \sigma)}{\sigma}\right)^2 \qquad (5)$$

From this analysis, it can be shown that the thickness of the implanted layer can be determined by the separation S of the fringe minima, and the compensation X by the fringe amplitudes:

$$t = (2Sn_f)^{-1} \quad ; \quad X = 1 - N_f/N_s = \frac{n_f(n_f^2-1)\sigma^2}{4\sigma^2_{p,s}}(R^2_{D,max}-1) \qquad (6)$$

The carrier concentration of the substrate may also be determined optically by measuring the reflectivity of an unimplanted sample and noting the wavenumber at which the reflectivity dips to a minimum at the edge of the plasma resonance. (ref. 6) At this wavenumber, the dielectric function of the film is very nearly 1. Again neglecting losses, the equation expressing this condition is easily solved for the carrier concentration:

$$N = \sigma_m^2(K_L-1)(2\pi c)^2\varepsilon_o m^*/e^2 \qquad (7)$$

The more heavily doped the sample is, the more the minimum moves to longer wavenumbers. This technique is sensitive for doping levels on the order of $10^{18}/cm^3$. For example, when $N=2x10^{18}/cm^3$, $\sigma_m=480\ cm^{-1}$;whereas for $N=4x10^{18}/cm^3$, $\sigma_m = 679\ cm^{-1}$. This difference in wavenumber is easily resolved by a spectrophotometer.

The measurements described above were made on a Perkin-Elmer Model 180 double beam infrared spectrophotometer fitted with dual specular reflectance attachments. As shown in table 1, the compensated layers are roughly 3 microns thick. Although the LSS theory predicts about 1 micron of penetration for each 100 keV of accelerator energy, some dose dependence is observed. The low values of the standard deviation, σ_t, are due to the periodicity of the fringes, which in turn indicates the ion-implanted layers can be modeled as dielectric slabs. The determination of the compensation from the reflectivity data is less straight forward. In general, the fringe amplitudes build up at a different rate than can be accounted for by the dielectric model, even in its exact formalism. The values reported represent the average value obtained. The fractional compensation was about 41% for the $10^{13}/cm^2$ implant and began to show saturation with a dose of $10^{14}/cm^2$. Saturation is clearly evident in the samples implanted to 10^{15} and $10^{16}/cm^2$. The standard deviations, σ_x, are larger in this case, due to the larger uncertainties in the reflectivities and the anomaly in the rate of fringe growth. The last two columns of table 1 show the

calculated carrier concentration of the films and the refractive indices at 10.6 microns, respectively. The refractive index of the sample implanted to $10^{16}/cm^2$ is very close to the literature value of 3.275 for undoped GaAs at 10.6 microns. (ref.7)

INFRARED OPTICAL WAVEGUIDING

Since the reflectivity spectra are interpretable in terms of a single dielectric film/substrate structure, the equations for a planar asymmetric dielectric waveguide were used as the waveguide model: (ref. 8)

$$kt\sqrt{n_f^2-(\beta/k)^2} - \Phi_{fo} - \Phi_{fs} = m\pi \tag{8}$$

where $k=2\pi/\lambda_o$, $\beta/k=n_f\sin\theta_f$ and the phase angles are defined by:

$$\tan \Phi_{fi}^{TE} = \left(\frac{(\beta/k)^2-n_i^2}{n_f^2-(\beta/k)^2}\right)^{\frac{1}{2}} \quad ; \quad \tan \Phi_{fi}^{TM} = (n_f/n_i)^2 \tan \Phi_{fi}^{TE} \tag{9}$$

The subscript i refers to either the cover layer o or to the substrate s. Equation (8) is the familiar eigenvalue condition which must be satisfied for optical waveguiding to occur and is expressed in terms of the ratio β/k. This factor can be interpreted as the effective refractive index of the waveguide for each mode and is restricted to values between n_s and n_f.

Infrared optical waveguiding was achieved in these samples using a 1 watt CO_2 laser operating at 10.6 microns. The radiation was focused through an f-10 ZnSe lens on a dove shaped germanium prism which effected coupling into and out of the waveguide. The emerging beam, totally internally reflected from the base of the prism, was imaged as a spot on a thermographic screen. Waveguiding was identified by an absorption notch in the reflected spot, indicating that radiation was removed from the incident beam. Measurements of the angles at which synchronous coupling was achieved were made for both s and p polarizations of the incident beam. From these angles, the effective indices of the guided modes were determined. As two modes were found, it was possible to numerically invert the mode equations to obtain the refractive index and thickness of the implanted layer.

The results of preliminary waveguiding measurements at 10.6 microns are shown in table 2. Due to experimental limitations discussed below, synchronous coupling was only achieved in the two more heavily doped samples, and in those only the 0-order modes were observed although it is believed those samples will also support the TE_1 mode.

The thickness obtained for sample 0519-7 is considerably larger than that obtained by IR reflectivity, although the values obtained for the refractive index compare well. With sample 0519-4 the agreement is better. The thickness obtained from the waveguide measurement is closer to that obtained by IR reflectivity while the values obtained for the refractive index are identical.

Figures 2 and 3 present these results in a different format. These are computer generated plots of the predicted mode structure for a planar asymmetric dielectric waveguide using as inputs for n_f and n_s values obtained from the IR reflectivity spectra. The TE modes are indicated by the solid curves, while the TM modes are represented by the dashed ones.

A horizontal line has been drawn on each figure at the thickness determined by the IR fringe analysis. The effective indices of the modes supported by each sample would be expected to be at the intersection of the mode curves with these lines, as indicated by the Δ symbols on the figures. The corresponding points obtained by the synchronous coupling measurements are shown by the + symbols.

For sample 0519-4 the measured modes are both obtained at larger values of β/k than expected and their separation is smaller, implying they intersect the mode curves at a larger value of thickness. That the waveguide data points remained on the mode curves indicates that the values of the refractive index obtained for the film by both methods are in excellent agreement.

Another point to be made from figure 2 is that regardless of which value is used for the guide thickness, the TE_1 mode should be supported by this sample. The germanium prism used in these experiments had an angle of 54 degrees which limited the lowest value of β/k obtainable to about 2.7. Another prism is being prepared so the entire range of β/k will be accessible. If the TE_1 mode is observed, the extra data point will provide more information about the actual refractive index profile.

The last feature to be noted from this figure is that the mode curves are bounded, in β/k, from n_s to n_f. The refractive index of the substrate for all the samples is 2.44 and is determined by the initial doping level of the GaAs. The refractive index of the film is determined by the carrier concentration remaining after implantation. It must therefore lie somewhere between 2.44 and 3.275, the value for undoped GaAs. Thus as the implant dose is decreased, the mode curves are all squeezed to the left as the upper limit on β/k decreases.

Figure 3 presents the same data for sample 0519-7. The spacing between the TE_o and TM_o modes indicates the layer is considerably thicker than predicted by IR reflectivity. That the mode curves are displaced slightly to the left of the theoretical curves illustrates the lower value of n_f obtained by the synchronous coupling measurements. This sample should also support the TE_1 mode and possibly the TM_1 mode.

DISCUSSION

Several conclusions can be deduced from these results. The first of these is that proton implantation done at the moderate energy of 300 keV produces a damage layer which will support optical waveguiding at 10.6 microns. Although these layers are very thin relative to the wavelength used, the index change produced is so large that the waveguiding condition is easily satisfied. This layer also appears to have very uniform optical properties since empirical results are explainable in terms of elementary models.

There is also very good agreement between the IR reflectivity results and the coupling measurements, indicating the experimentally easier reflectivity analysis has considerable predictive utility. Although it is not fully apparent from the data presented here, it has been found that these are probably complimentary techniques: IR reflectivity appears to be more sensitive to the thickness of the layer than to the refractive index while the coupling measurements yield greater uncertainty in the thickness of the layer and very small standard deviations in the refractive index. It is expected that the refractive index profile of ion-implanted waveguides will be shown to have a transition region between the guiding layer and the substrate rather than a sharp discontinuity as assumed in the models presented

here. The complimentarity of the measurement techniques, as well as the systematic differences in the experimental results, may be explained by the different way light experiences the transition region in each of these techniques.

Finally it is noted that the effective indices of the guided modes are strongly dependent on dose, which is easily controlled. This suggests that structures requiring different velocities of propagation, such as delay lines, can be fabricated simultaneously on the same substrate through proper control of the ion beam.

The measurements reported here were made on as-implanted samples. While current work is directed at completing these coupling experiments, the question of losses and post implantation processing to minimize them will be addressed.

REFERENCES

1. Barnoski, M. K.: Introduction to Integrated Optics. Plenum, NY, 1974.

2. Garmire, E., Stoll, H., Yariv, A., and Hunsperger, R. G.: Optical Waveguiding in Proton-Implanted GaAs. Appl. Phys. Lett., vol. 21, no. 3, 1 August 1972, pp. 87-88.

3. Kachare, A. H., Spitzer, W. G., Frederickson, J. E., and Euler, F. K.: Measurements of Layer Thicknesses and Refractive Indices in High-Energy Ion-Implanted GaAs and Gap. J. Appl. Phys., vol. 47, no. 12, Dec. 1976, pp. 5374-5381.

4. Zavada, J. M., Jenkinson, H. A., and Gavanis, T. G.: Optical Properties of Proton Implanted n-type GaAs. SPIE Proceedings, Vol. 276, 1981, pp. 104-108.

5. Gibbons, J. F., Johnson, W. S., and Mylroie, S. W.: Projected Range Statistics. Dowden, Hutchinson & Ross, Inc., Stroudsburg, 1975.

6. Goldsmith, N., and Oshinsky, W.: Vapor-Phase Synthesis and Epitaxial Growth of Gallium Arsenide. RCA Review, vol. 24, Dec. 1963, pp. 546-554.

7. Cheo, P. K., and Wagner, R.: Infrared Electrooptic Waveguides. IEEE J. Quant. Elect., vol. QE-13, no. 4, April 1977, pp. 159-164.

8. Tien, P. K.: Light Waves in Thin Films and Integrated Optics. Applied Optics, vol. 10, no. 11, Nov. 1971, pp. 2395-2413.

TABLE 1.-CHARACTERIZATION OF SAMPLES BY INFRARED REFLECTIVITY
AS-IMPLANTED: 300 keV H^+ @ ROOM TEMPERATURE

SAMPLE	DOSE $1/cm^2$	t μm	σ_t μm	X	σ_X	N_f $1/cm^3$	n_f (@10.6μ)
0519-1	10^{13}	2.64	.06	.41	.10	2.2×10^{18}	2.79
0519-5	10^{14}	3.05	.07	.57	.22	1.8×10^{18}	2.94
0519-7	10^{15}	3.35	.02	.93	.12	2.8×10^{17}	3.22
0519-4	10^{16}	3.31	.01	.98	.19	6.8×10^{16}	3.26
SUBSTRATE						3.8×10^{18}	2.44

TABLE 2.-CHARACTERIZATION OF SAMPLES BY CO_2 LASER WAVEGUIDING
AS-IMPLANTED: 300 keV H^+ @ ROOM TEMPERATURE

SAMPLE	DOSE $1/cm^2$	MODE	β/k	t μm	n_f
0519-7	10^{15}	TE_o	3.071	4.54	3.20
		TM_o	3.026		
0519-4	10^{16}	TE_o	3.087	3.71	3.26
		TM_o	3.014		

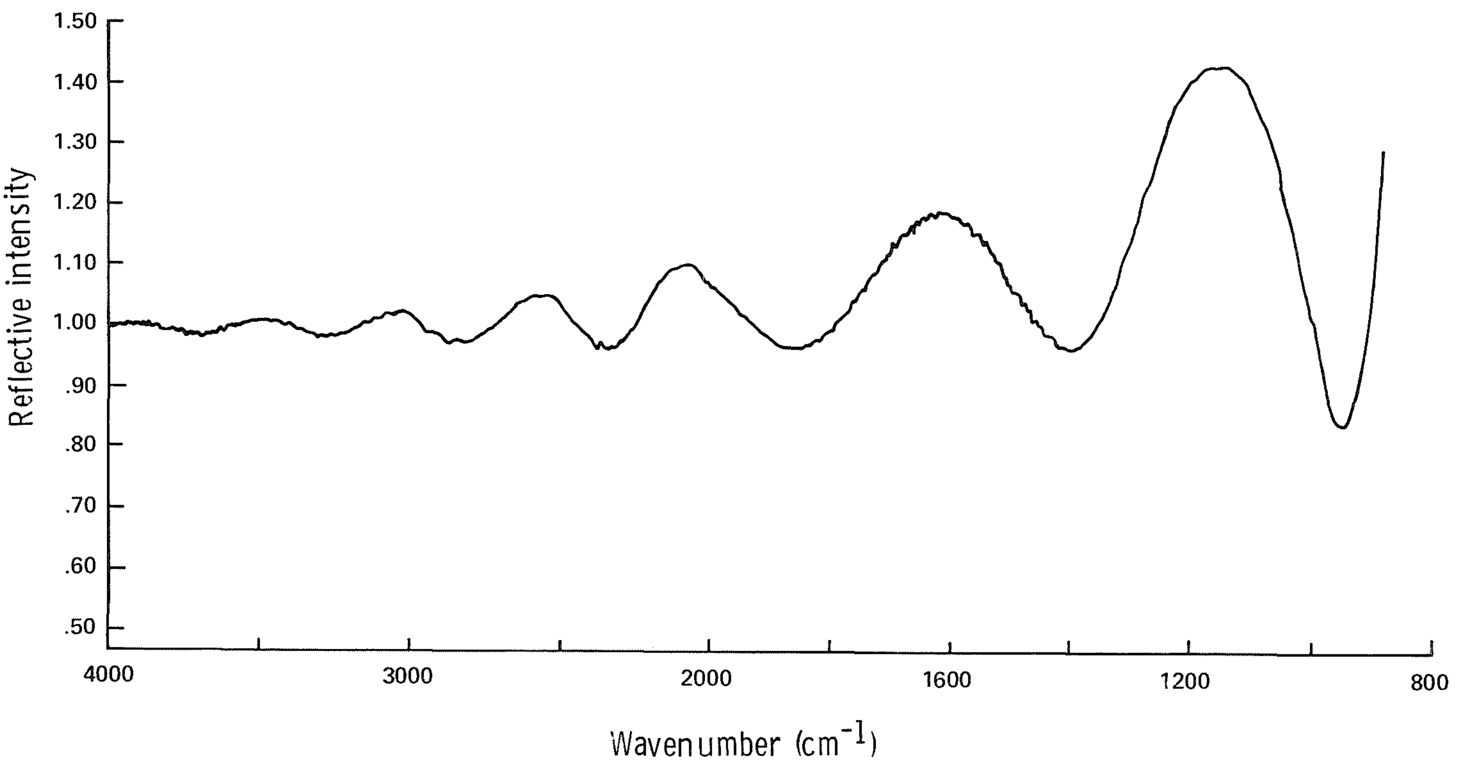

Figure 1.- Differential reflectivity spectrum of sample GaAs 0519-4 (10^{16} H^+/cm^2).

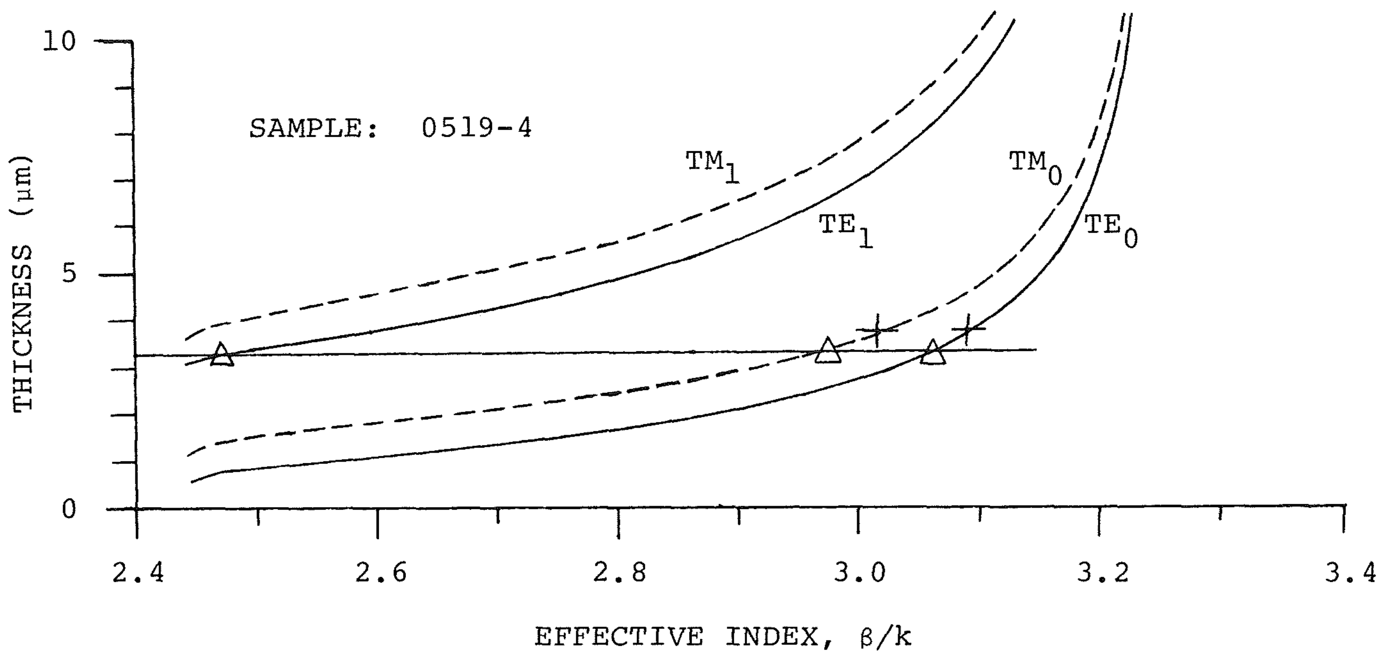

Figure 2.- Comparison of waveguiding and reflectivity results for sample GaAs 0519-4(10^{16} H^+/cm^2). Curves and points indicated by the symbol Δ are predictions based on IR fringe analysis. Results of waveguiding experiments are indicated by the + symbol.

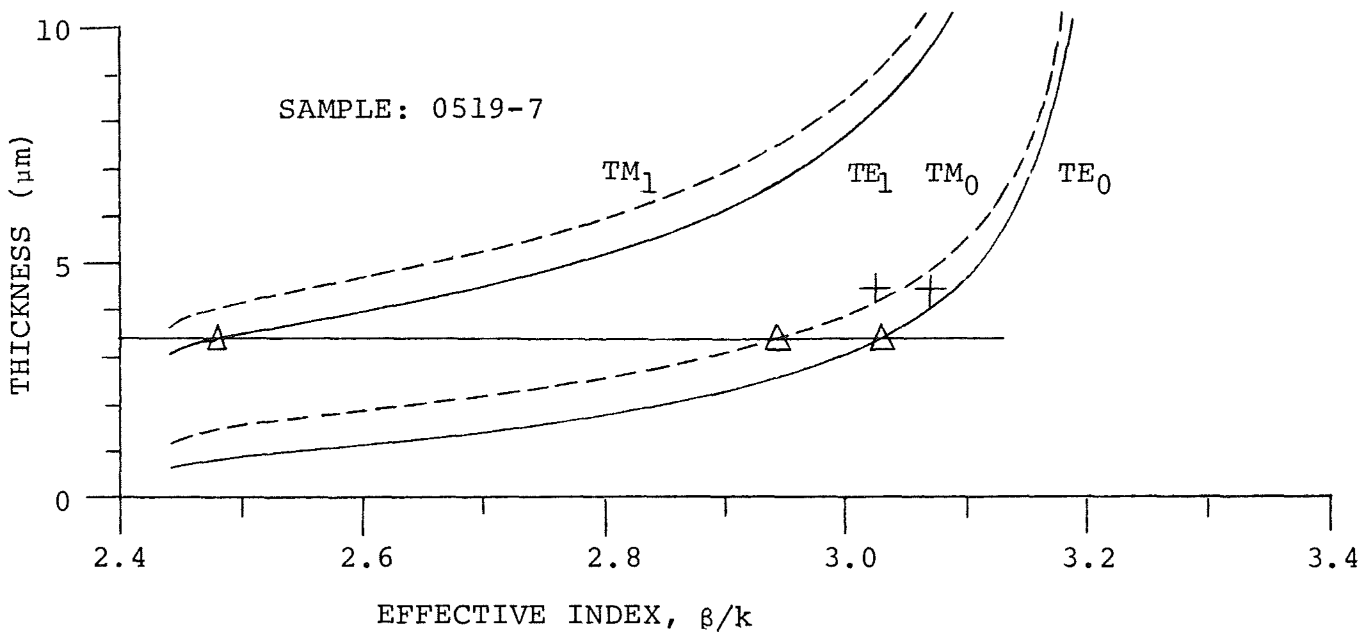

Figure 3.- Comparison of waveguiding and reflectivity results for sample GaAs 0519-7(10^{15} H^+/cm^2). Curves and points indicated by the symbol Δ are predictions based on IR fringe analysis. Results of waveguiding experiments are indicated by the + symbol.